LETTER *Earth Planets Space*, **60**, 127–132, 2008

Tsunami generated by the 2007 Noto Hanto earthquake

Yuichi Namegaya and Kenji Satake

Active Fault Research Center, Geological Survey of Japan, National Institute of Advanced Industrial Science and Technology, 1-1-1 Higashi, Tsukuba 305-8567, Japan

(Received July 2, 2007; Revised October 11, 2007; Accepted October 23, 2007; Online published February 19, 2008)

Tsunami numerical simulations of the 2007 Noto Hanto earthquake are carried out for three models based on the coastal vertical movements, the GPS observations, and the strong-motion data. The three fault models produce similar tsunami waveforms at five tide gauge stations around the source. Comparisons with the observed tsunami waveforms indicate that the fault model based on the coastal movements shows the best agreement but that a slightly smaller fault area with a larger slip amount would make the agreement better. At three tide gauge stations in Toyama Bay, unusual oscillatory waves were recorded before the expected tsunami arrival. The spectral analysis of the observed records indicates that they represent characteristic oscillation of Toyama Bay, and modal calculations show that they can be reproduced by the water displacement in the mouth of Nanao Bay generated by a possible extension of the mainshock fault toward the southeast or a possible landslide source at a steep part of ocean bottom.

Key words: The 2007 Noto Hanto earthquake, tide gauge records, tsunami numerical simulation, fault models, oscillation of Toyama Bay.

1. Introduction

On 25 March 2007, a large earthquake occurred off the north-western coast of Noto peninsula, Japan (Fig. 1(a)). The source parameters provided by the Japan Meteorological Agency (JMA) are as follows: origin time, 09:41:58 (JST); epicenter, 136°41′16″E and 37°13′24″N; depth, 10.7 km; magnitude, 6.9. The focal mechanism (strike, dip, rake) and the seismic moment are estimated as (58°, 66°, 132°) and 1.36×10^{19} N m by the F-net of NIED (National Research Institute for Earth Science and Disaster Prevention, Japan), and as (58°, 60°, 117°) and 9.1×10^{18} N m by USGS. The earthquake had a predominantly thrust fault motion with high dip-angle and some right-lateral strike-slip component. The earthquake generated a small tsunami. The maximum heights of the tsunami recorded at the tide gauge stations were 23 cm (at 11:14) at Noto and 16 cm (at 12:22) at Kanazawa port.

Many fault models of the earthquake have been proposed by various researchers using different kinds of data. Among them, we introduce three representative models estimated by different kinds of data. The first model, by Awata *et al.* (2008), is based on the coastal movements measured within about 4 weeks of the mainshock. They measured the upper heights of the oysters on the quay walls and estimated the vertical movements at each coastal location. Assuming a rectangular fault plane (15 km × 12 km) with a uniform slip (1.2 m), they found that the calculated coastal movements, using a dislocation model (Okada, 1992), are in good agreement with the observed ones (Fig. 1(b)). The second model, by the Geographical Survey Institute (GSI) (2007), is based on GPS data. The GSI also proposed a rectangular fault plane (21.2 km × 13.9 km) with a uniform slip (1.65 m) (Fig. 1(c)). The last model, by Horikawa (2008), is based on the strong-motion data recorded at six stations of K-Net, one station of KiK-net, and one station of JMA. The fault model consists of 440 subfaults, 1 km × 1 km in size and 22° in strike direction and 20° in dip direction. The largest slip was estimated as about 2.75 m (Fig. 1(d)). Hereafter, we call the above three models of Awata *et al.* (2008), GSI (2007), and Horikawa (2008) as the CM (Coastal Movement), GPS, and SM (Strong Motion) models, respectively. Figure 1(b–d) indicates that the GPS model produces the largest western extension of ground deformation and that the SM model produces the largest southern extension. The maximum uplift of ground surface is calculated as about 0.6 m for the GPS model, about 0.5 m for the CM model, and about 0.4 m for the SM model.

The major aim of this paper is to compute tsunami waveforms at coastal tide gauge stations using the above three models and to compare these with the observed ones. As we will describe in the next section, tide gauge records in Toyama Bay show oscillatory waves soon after the earthquake but before tsunami arrival. The second aim of this paper is to examine these waves in terms of characteristic oscillation of Toyama Bay.

2. Observed Tsunami Records

In order to examine the tsunami from the Noto Hanto earthquake, we collected 37 tide records along the Japan Sea coast, from Hokkaido to western Honshu (Fig. 1(a)). Most tide gauge records, unfortunately, did not record clear tsunami signals; either the noises are too large or the tsunami signals are not clear. Of these, we use five tide

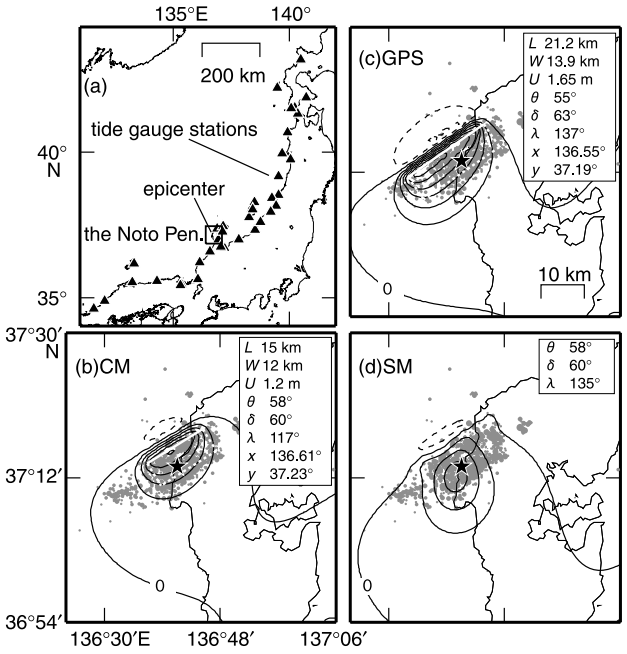

Fig. 1. (a) Station locations (triangles) where we collected tide gauge records. The rectangle indicates the area shown in (b)–(d). (b) The vertical ground deformation of the Coastal Movement (CM) model. The solid and dashed contours indicate uplift and subsidence, respectively. The contour interval is 0.1 m. The white rectangle shows the surface projection of fault plane whose parameters are shown in the upper right box. The symbols of L, W, U, θ, δ, λ, x, y, and d denote length, width, slip, strike, dip, rake, longitude, latitude, and depth of the upper-left of the fault, respectively. The solid line of the white rectangle indicates the upper side. The star is the mainshock epicenter. The gray circles are the aftershocks within 24 h of the mainshock after JMA. (c) The same for the GPS model. (d) The same for the Strong Motion (SM) model.

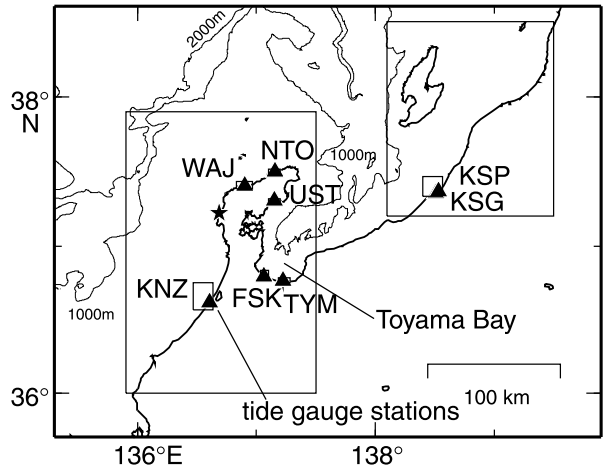

Fig. 2. Tide gauge stations (triangles) whose records are used in this paper. See text or Fig. 3 for the full names of stations. The star symbol denotes the mainshock epicenter. The tsunami simulations are carried out in the map region using the bathymetry shown. The interval of the bathymetry contour line is 1,000 m. Rectangles show the areas where nested grids are adopted.

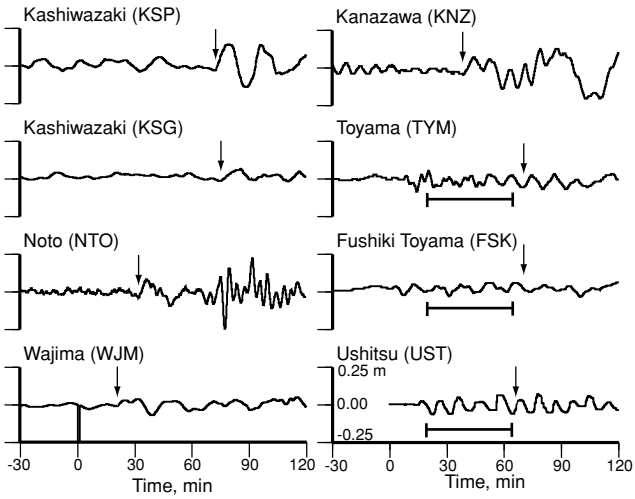

Fig. 3. The records at the tide gauge stations shown in Fig. 2. The astronomical tide is removed. The time origin is the mainshock origin time. The arrows for KSP, KSG, NTO, WJM, and KNZ are the observed tsunami arrival times, and those for TYM, FSK, and UST are estimated by the tsunami simulation for the CM model. The belts in the records of TYM, FSK, and UST indicate the time range in which we carried out the spectral analysis in Section 4.

records for the estimation of the source models (Fig. 2). These are Kashiwazaki (KSP) operated by Niigata prefecture, Kashiwazaki (KSG) operated by GSI, Noto (NTO) operated by JMA, Wajima (WJM) operated by GSI, and Kanazawa (KNZ) operated by Ministry of Land, Infrastructure and Transport Government of Japan (MLIT). The distance between stations KSP and KSG is about 2 km, and the latter is located west-southwest of the former. In addition, we note that three tide records in Toyama Bay recorded the oscillation of sea levels immediately after the earthquake. These are Toyama (TYM) operated by JMA, Fushiki-Toyama (FSK) operated by MLIT, and Ushitsu (UST) operated by Ishikawa prefecture (Fig. 2). We analyzed these records to examine the cause of the oscillation. The sea level is digitally recorded with a sampling interval of 60 s at FSK, 30 s at KSG and WAJ, 15 s at NTO and TYM, and 6 s at KNZ. At KSP and UST, the sea levels were recorded in analog form, hence we digitized the records on the paper sheets.

The records of the above eight tide gauge stations are shown in Fig. 3. In order to compare the observed and calculated tsunami waveforms in later section, we here describe the characteristics of the observed tsunami arrival time and the amplitude of the first wave. At KSP, the tsunami arrival was recorded at 72 min after the earthquake and the first upward motion of 14 cm was recorded at 79 min. At KSG, the tsunami arrival and the first upward motion of 7 cm were recorded at 75 min and 86 min after the earthquake, respectively. At NTO, the tsunami arrival and the first upward motion of 9 cm were recorded at 32 min and 36 min after the earthquake, respectively. At WJM, the tsunami arrival and the first upward motion of 3 cm were recorded at 21 min and 25 min, respectively. At KNZ, the tsunami arrival and the first upward motion of 7 cm were recorded at 39 min and 44 min, respectively.

At three tide gauge stations in Toyama Bay (UST, FSK, and TYM), the water waves with the period of about 10 min, similar to that of the tsunami wave, were recorded immediately after the earthquake, before the arrival of the computed tsunami.

3. Modeling Tsunami Waveforms

We calculate the tsunami waveforms at five tide gauge stations (KSP, KSG, NTO, WJM, and KNZ) using the three initial conditions derived from the CM, GPS, and SM models, and compare them with the observed ones. The finite-difference computations of the shallow-water wave equations are carried out on the spherical coordinate system (see Satake, 1995). The computational area is from 135°18′ to 139°54′E and from 35°42′ to 38°36′N, as shown in Fig. 2. The grid size is 20 s of the arc (617 m along the meridian), but around tide gauge stations we use the finer grid size of 6.7 (20/3) s and 2.2 (20/9) s. In the areas with the finest grid, we compute the nonlinear shallow-water wave equations with advection terms and a bottom friction with non-dimensional frictional coefficient of 0.003. In the other areas with coarser grids, we compute the linear long-wave equations. The effect of the Coriolis force is neglected in the whole area. For the connections between the coarse and fine grids, we use an interpolation method proposed by Aida (1978). At the boundary between sea and land, the flux (velocity) normal to the boundary is set at zero. At the seaward boundary of the computing area, we use the radiation condition (e.g., Aida, 1969). For the computational stability, sea depth shallower than 2 m is set at 2 m, and the time interval of finite-difference computation is set at 0.1 s. Although we adopt the nonlinear shallow-water equations in the finest grid, we note that the first cycle or two of the calculated tsunami waveforms by nonlinear and linear equations are almost identical at most stations.

We use the bathymetric data of the JTOPO30 and M7000 series provided by Marine Information Research Center, Japan Hydrographic Association. We read the locations of the breakwaters from the topographic map of 1:25,000 provided by GSI, and the locations are included in the bathymetric data.

Figure 4 shows the comparisons of the calculated tsunami waveforms from the three models with the observed ones at the five tide gauge stations. Here, we compare the calculated waveforms with the observed ones in terms of the period (waveform), the arrival time, and the amplitude of the first wave, for the purpose of the examination of the fault models.

We find that the calculated waveforms are generally similar to each other regardless of the model, and they are also similar to the observed ones. This indicates that the three fault models based on different kinds of data can basically explain the observed tsunamis.

In terms of the arrival times, the calculated ones from the three models are nearly equal to the observed ones at KSG and NTO. At KSP, however, the calculated arrival times from the three models are about 10 min later than the observed one. Since the calculated waveforms are similar to the observed one and the observed waveform was recorded on the paper sheet in analogue form, the disagreement may be due to a timing error. At WJM, the calculated arrival times from the three models are earlier than the observed one by about 3 min. At KNZ, the only station located in the southwestern direction of the mainshock source area, the calculated arrival times from the CM, GPS, and SM models are about 6 min, 12 min, and 18 min earlier than the observed one, respectively. These indicate that, while the CM model is the closest to the actual tsunami source, all three fault models have larger southern or western extensions than the actual one and that the fault length should be shortened to better match the tsunami first arrival at KNZ.

In terms of the first wave amplitude, at KSP, KSG, and

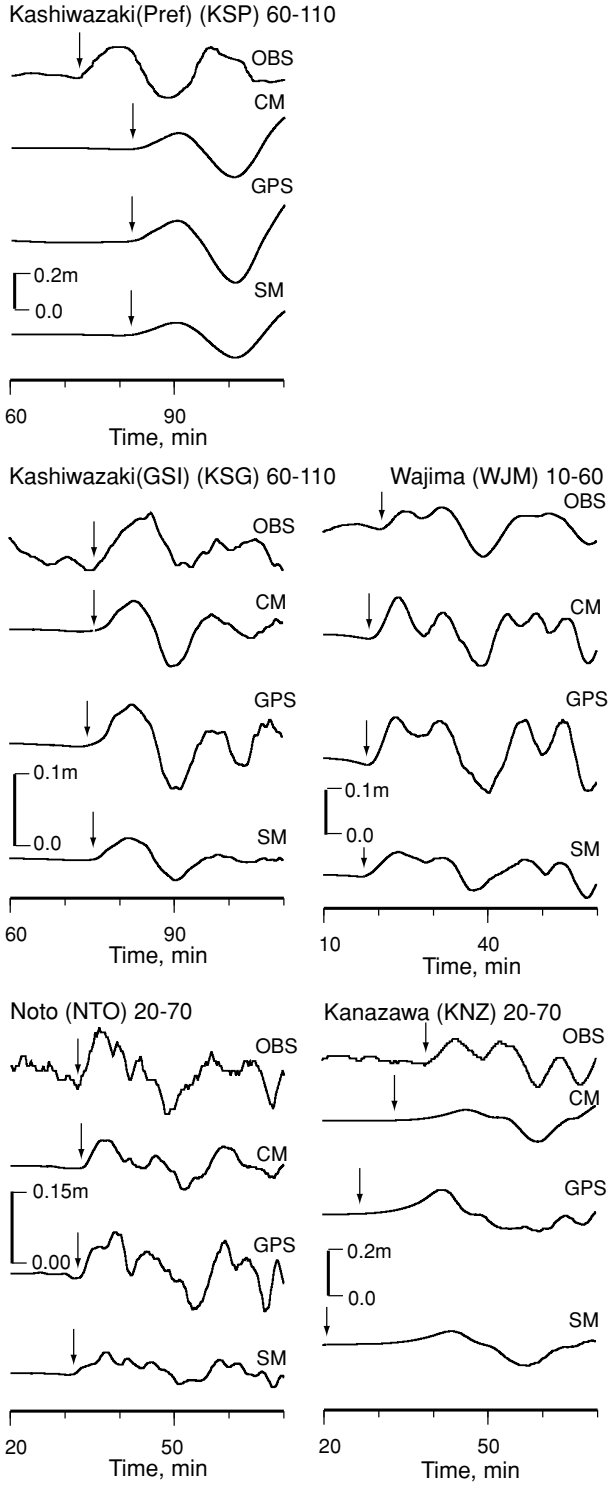

Fig. 4. Comparison of the observed tsunami waveforms with those calculated from the CM, GPS, and SM models. Note the different amplitude scales for different stations. Numbers next to the station names indicate the time window (min from the earthquake origin time) of the waveforms. The arrows are the tsunami arrival times judged by us.

NTO, the calculated ones from the CM and SM models are smaller than the observed ones, while the calculated ones from the GPS model are nearly equal to or slightly smaller than the observed. At WJM, the calculated amplitudes from the CM and GPS models are about twofold larger than the observed one, while the calculated one from the SM model is nearly equal to the observed one. At KNZ, the amplitudes from the CM and GPS models are smaller and larger than the observed one, respectively, while that from the SM model is nearly equal to the observed one. In summary, the calculated amplitudes from the CM model are smaller than the observed ones at each station except for WJM. Those from SM model are smaller than or equal to the observed ones, and those from the GPS model are similar to the observed ones at some stations, but larger than the observed ones at the other stations.

The above comparisons of arrival times and first wave amplitudes indicate that the tsunami source area is slightly smaller than that of the CM model, but the slip amount is slightly larger than that of the CM model.

4. Oscillation in Toyama Bay

The tide gauge records of UST, FSK, and TYM, all located in Toyama Bay, show unusual oscillatory waves before the arrival of the tsunami generated from the mainshock fault model (Fig. 3). The period of this oscillation is about 10 min, and the amplitude is several centimeters. The oscillation lasted for more than 40 min and continued after the arrival of the tsunami propagated around Noto Peninsula. Abe *et al*. (2008) proposed that a landslide triggered by earthquake ground motion in Toyama Bay caused the oscillations. They estimated the landslide location based on an inverse refraction diagram drawn from a few wave gauges in Toyama Bay.

If the long-lasting oscillatory waves represent the characteristic oscillation of Toyama Bay, they can be expressed as a superposition of characteristic oscillation modes (e.g., Satake and Shimazaki, 1987, 1988). We therefore carry out spectral analysis of the three tide records. We estimate power spectra of each record, coherences and phase differences between the three pairs (Fig. 5) from the 47-min records before the tsunami arrival (Fig. 3). The power spectra indicate that the dominant period of the oscillation at UST and TYM is 11.4 min, that the coherence between these two stations is significant (0.6), and that the phase is in opposite sense (the difference is about 180°). The dominant period at FSK is 13.7 min, and coherences with the other two stations are nearly zero. From these analyses, we hypothesized that (1) the UST and TYM records indicate the same oscillation mode, but this mode is not recorded at FSK; (2) the FSK record represents another mode which is not recorded at UST and TYM.

In order to estimate the characteristic oscillation modes of Toyama Bay, we calculate the normal modes using the method of Loomis (1975). Based on the bathymetry data of Toyama Bay with grid size of 1.7 km × 1.7 km, we calculate the first 100 modes (Fig. 6(a)).

Which of the above 100 modes do the observed spectral peaks represent? Generally, when the initial water height distribution $h_0(x, y)$ is given in a closed or semi-closed basin, the tsunami waveforms $h(x, y, t)$ can be expressed as a superposition of the eigenvectors $\Phi_k(x, y)$ of the kth characteristic oscillation, since the eigenvectors form a complete orthogonal set (see Satake and Shimazaki, 1987). Here, the kth eigenvector indicates the amplitude distribution of the kth oscillation mode. The tsunami waveforms $h(x, y, t)$ are then expressed as

$$h(x, y, t) = \sum_k C_k \Phi_k(x, y) \cos \omega_k t \qquad (1)$$

where ω is characteristic angular frequency, and the subscript k denotes the kth mode. The coefficient or weight C_k is determined from the initial water height distribution $h_0(x, y)$ by using the orthogonality of the eigenvectors,

$$C_k = \iint_S h_0(x, y) \Phi_k(x, y)\, dxdy \qquad (2)$$

where S indicates the area of the closed or semi-closed basin. The weights C_k show which mode in the bay is excited by the given initial water height distribution.

We then calculate the weights of each mode, C_k, for a small source located in Nanao Bay (A in Fig. 6(c–e)) whose size is 1.7 km × 1.7 km (one grid size) with a uniform water height of 0.2 m (Fig. 6(b)). This implies either a southeastward extension of the ground deformation due to faulting or a landslide occurred at a steep part of Nanao Bay. The relative size of the weights (Fig. 6(a)) is in good agreement with that of the observed spectra. Figure 6(c–e) shows the oscillation patterns, or eigenvectors, of some of the modes close to the observed dominant periods: the 40th (13.3 min), 54th (11.4 min), 56th (11.1 min) modes.

For the 40th mode (Fig. 6(c)), the amplitude is relatively large at FSK and small at UST and TYM. This explains hypothesis (2), and indicates that the 40th mode may correspond to the observed dominant peak of 13.7 min. For the 54th mode (Fig. 6(d)), which has the largest C_k (Fig. 6(a)), the amplitude at Nanao Bay is the maximum value (1.0) of the eigenvector, hence this mode can be easily excited. However, the relative amplitudes are small at all three stations, and therefore they may not be observed. For 56th

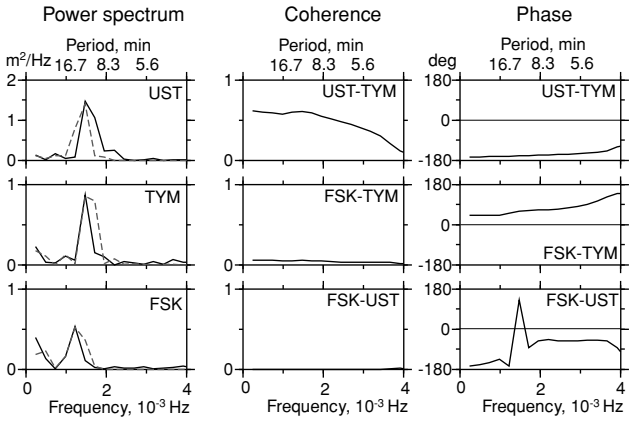

Fig. 5. Spectral analysis at UST, TYM, and FSK stations of the tide records (solid lines). The left, center, and right columns correspond to the power spectra, coherences, and phase differences, respectively. The dashed lines indicate the power spectra of synthetic waveforms derived from the initial water displacement in the mouth of Nanao Bay.

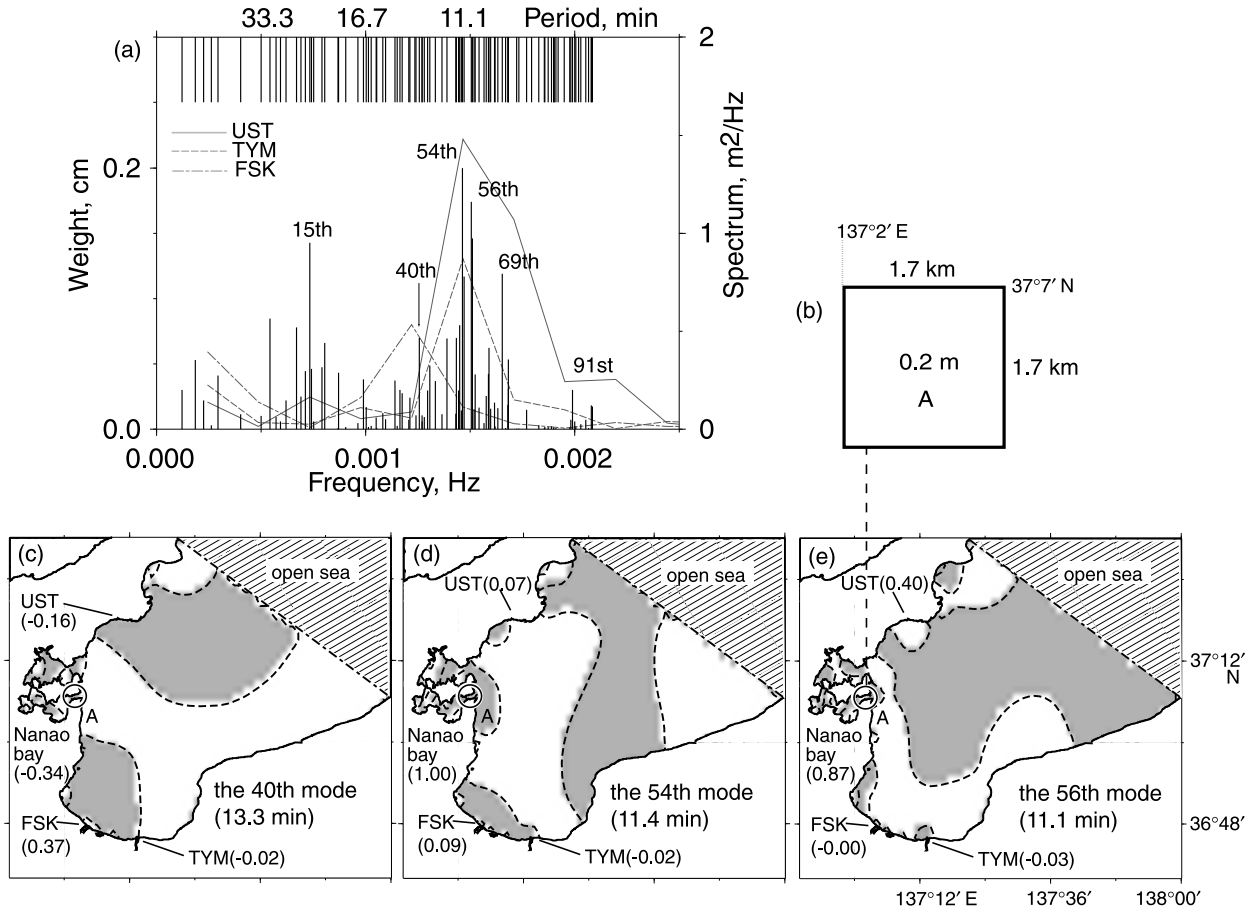

Fig. 6. (a) (top) Characteristic periods of the first 100 modes calculated by the method of Loomis (1975). (bottom) The gray solid, dash, and dot-and-dash lines denote the power spectra of the UST, TYM, and FSK records taken from Fig. 5. The vertical bars show the weights of the modes C_k calculated for an initial condition shown in (b). (c) The characteristic oscillation pattern, or eigenvector Φ of the 40th mode in Toyama Bay. The dashed lines indicate the nodal lines, and the phase in the gray region is opposite to that of the white region. Prescribed open boundary is also shown (dot-and-dash lines). Numbers at UST, Nanao Bay, FSK, and TYM indicate relative amplitudes normalized by maximum of eigenvectors Φ_k for each mode. (d) The characteristic oscillation pattern of the 54th mode. (d) The characteristic oscillation pattern of the 56th mode.

mode (Fig. 6(e)), the eigenvector shows a large relative amplitude at UST, a small amplitude at TYM, a nearly zero amplitude at FSK, and the opposite sign for UST and TYM. These satisfy hypothesis (1) and indicate that this mode may be a part of the observed dominant peak at UST and TYM.

In addition, we compute the spectra of the synthetic waveforms derived from Eqs. (1) and (2) by using the initial uniform height in the mouth of Nanao Bay (Fig. 5). The spectra are in good agreement with the observed ones. This result indicates that the unusual waves in tide gauge records in Toyama Bay before the expected tsunami arrival can be reproduced by characteristic modes excited by a small initial displacement in Nanano Bay with a volume of 5.8×10^5 m^3 (1.7 km $\times$ 1.7 km $\times$ 0.2 m).

5. Conclusion

The tsunami numerical simulations of the 2007 Noto Hanto earthquake and comparisons with the observed tsunami waveforms at the five tide gauge stations (two at Kashiwazaki, Noto, Wajima, and Kanazawa) indicate that the CM model, based on the coastal movements (Awata *et al.*, 2008), shows a better agreement than the GPS model (GSI, 2007) or the SM model based on the strong-motion data (Horikawa, 2008). Careful comparisons of the arrival times and the amplitudes of the first waves indicate that the tsunami source area is slightly smaller than and the slip amount is slightly larger than those of the CM model.

At the three tide gauge stations in Toyama Bay (Ushitsu, Toyama and Fushiki), oscillatory waves similar to the tsunami were recorded immediately after the earthquake and continued after the tsunami arrival around Noto peninsula. The spectral analysis of the observed records and the calculation of characteristic oscillation modes of Toyama Bay indicate that the observed oscillations are reproduced if a small source (volume 5.8×10^5 m^3) is located in the mouth of Nanao Bay, as a result of either a southeastward extension of the ground deformation due to faulting or a landslide occurred at a steep part of the bay.

Acknowledgments. We thank the Japan Meteorological Agency, Geographical Survey Institute Japan, Ministry of Land, Infrastructure and Transport Japan, Niigata prefecture, and Ishikawa prefecture for providing us their tide gauge records. We used bathymetry data compiled and provided by the Japan Hydrographic Association and Geographical Survey Institute, Japan. Dr. Y. Tanioka and an anonymous reviewer provided us valuable comments that improved the paper. Dr. H. Horikawa provided us his source models (slip distribution). Most of the figures were generated by using General Mapping Tools (Wessel and Smith, 1998).

References

Abe, I., K. Goto, F. Imamura, and K. Shimizu, Numerical simulation of the tsunami generated by the 2007 Noto Hanto Earthquake and implications for unusual tidal surges observed in Toyama Bay, *Earth Planets Space*, **60**, this issue, 133–138, 2008.

Aida, I., Numerical Experiments for the Tsunami propagation—the 1964 Niigata Tsunami and the 1968 Tokachi-oki tsunami, *Bull. Earthq. Res. Inst. Univ. Tokyo*, **47**, 673–700, 1969.

Aida, I., Reliability of a tsunami source model derived from fault parameters, *J. Phys. Earth*, **26**, 57–73, 1978.

Awata, Y., S. Toda, H. Kaneda, T. Azuma, H. Horikawa, M. Shishikura, and T. Echigo, Coastal deformation associated with the 2007 Noto Hanto earthquake, central Japan, determined by uplifted and subsided intertidal organisms, *Earth Planets Space*, 2008 (in press).

Geographical Survey Institute, The fault of the Noto Hanto Earthquake in 2007, http://cais.gsi.go.jp/Research/crust/notohanto/fault_model.html, 2007 (in Japanese).

Horikawa, H., Characterization of the 2007 Noto Hanto, Japan, earthquake, *Earth Planets Space*, 2008 (in press).

Loomis, H. G., Normal modes of oscillation of Honokohau harbor, Hawaii, *Hawaii Inst. Geophysics Univ. Hawaii*, **HIG-75-20**, 1–20, 1975.

Okada, Y., Internal deformation due to shear and tensile faults in a half-space, *Bull. Seismol. Soc. Am.*, **82**, 1018–1040, 1992.

Satake, K., Linear and nonlinear computations of the 1992 Nicaragua earthquake tsunami, *Pure Appl. Geophys.*, **144**, 455–470, 1995.

Satake, K. and K. Shimazaki, Computation of tsunami waveforms by a superposition of normal modes, *J. Phys. Earth*, **35**, 409–414, 1987.

Satake, K. and K. Shimazaki, Free oscillation of the Japan sea excited by earthquakes—II. Modal approach and synthetic tsunamis, *Geophys. J.*, **93-3**, 457–463, 1988.

Wessel, P. and W. H. F. Smith, New, improved version of the Generic Mapping Tools released, *EOS Trans. AGU*, **79**, 579, 1998.

Y. Namegaya (e-mail: yuichi.namegaya@aist.go.jp) and K. Satake